PAPER

Smart material concept: reversible microstructural self-regeneration for catalytic applications†

Dariusz Burnat,*[a] Roman Kontic,[a] Lorenz Holzer,[b] Patrick Steiger,[cd] Davide Ferri[c] and Andre Heel[a]

This paper presents a proof-of-concept study and demonstrates the next generation of a "smart" catalyst material, applicable to high temperature catalysis and electro-catalysis such as gas processing and as a catalyst for solid oxide cells. A modified citrate-gel technique was developed for the synthesis of $La_xSr_{1-1.5x}Ti_{1-y}Ni_yO_{3-\delta}$. This method allowed the synthesis of single phase materials with a high specific surface area, after the first calcination step at temperatures as low as 650 °C. Up to 5 at% of nickel could be incorporated into the perovskite structure at this low calcination temperature. X-ray powder diffraction and microscopy techniques have proven the exsolution of nickel nanoclusters under low oxygen partial pressure. The amount of exsoluted nickel nanoparticles was sensitive to surface finishing, whereby much more exsoluted nanoparticles were observed on pre-treated and polished surfaces as compared to original ones. Increasing A-site deficiency leads to a larger number of nickel particles on the surface, indicating a destabilizing influence of the A-site vacancies on the B-site metal cations. Repetitive redox cycles prove that the nickel exsolution and re-integration is a fully reversible process. These materials working in a cyclic and repetitive way may overcome the drawbacks of currently used conventional catalysts used for high temperature systems and overcome major degradation issues related to catalyst poisoning and coarsening-induced aging.

Introduction

Catalytically active nanoparticles are crucial for technologies related to catalysis and electro-catalysis because these particles ensure, with their high specific surface area, high turnover rates and drive process efficiency. The preservation of high catalytic activity is therefore of great significance. Supported noble metal catalysts suffer from particle sintering under high temperature reaction conditions and prolonged operation. Aging of the catalyst surface occurs in a two-fold way, over time.[1,2] On one hand, microstructural or morphological degradation, such as coalescence, leads to a loss of surface area. On the other hand, an even more rapid catalyst deactivation is caused by catalyst poisons, such as carbon or sulfur depositions, blocking the catalyst surface.[3] Both mechanisms typically lead to an irreversible loss of performance and require expensive material

recycling or even a complete replacement. Both effects lead to an economic drawback. Catalytically active nanoparticles are usually prepared using wet chemistry infiltration techniques. These, in turn, require additional processing steps and lead to excessive deposition of the catalytically active materials and the resulting nanostructured particles are susceptible to coalescence. A novel approach towards surface functionalization is the preparation of nanostructured particles, directly from a host matrix, which can occur under change of operating conditions.[4] A modification of this approach has led to some promising results, based on lanthanum doped perovskites $(A_xA'_{1-x}Ti_{1-y}Me_yO_{3-\delta}$, A: La, Y A': Ca, Sr, Mg). The B-site cations, *i.e.* Me = Fe, Ni, Cu, Mn, introduced into the perovskite lattice, were exsoluted from the host matrix, under low oxygen partial pressure, and remain on its surface as catalytically active particles.[5,6] Besides excellent thermal stability at elevated temperatures, a very good electronic conductivity is obtained, which makes them attractive for high temperature electro-catalysis. In this work, we demonstrate a more progressed smart material concept (Fig. 1) for a high temperature catalyst: exsolution, but also the subsequent reintegration of the catalytic metal phase into the host matrix. It is shown that this effect is reversible and can be used repetitively for microstructural self-regeneration, with the aim to use this mechanism even for the regeneration of the catalytically active phase suffering from process related poisons such as sulfur or carbon.

[a] ZHAW – Zurich University of Applied Sciences, IMPE – Institute of Materials and Process Engineering, Technikumstrasse 9, CH-8400 Winterthur, Switzerland. E-mail: dariuszartur.burnat@zhaw.ch

[b] ZHAW – Zurich University of Applied Sciences, ICP – Institute of Computational Physics, Technikumstrasse 9, CH-8400, Switzerland

[c] Paul Scherrer Institute PSI, 5232 VIlligen, Switzerland

[d] EPFL – Ecole Polytechnique Fédérale de Lausanne, ISIC – Institute of Chemical Sciences and Engineering, Switzerland

† Electronic supplementary information (ESI) available. See DOI: 10.1039/c6ta03417a

This journal is © The Royal Society of Chemistry 2016

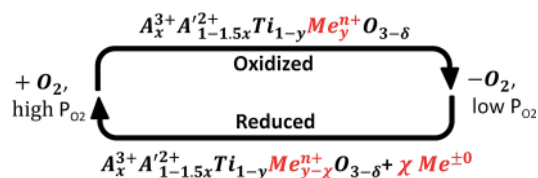*J. Mater. Chem. A*, 2016, **4**, 11939–11948 | 11939

Fig. 1 Smart material regeneration concept: catalyst nanoparticle exsolution and reintegration mechanism stimulated by redox cycling.

A-site deficient compositions, combining trivalent (A) and bivalent (A′) metal cations within the perovskite network, following the stoichiometry $A_x^{3+}A'^{2+}_{1-3/2x}Ti_{1-y}Me_yO_{3-\delta}$, are specifically addressed due to their suitable properties. In this proof-of-concept study, we selected nickel as the segregating and re-incorporating metal due to its catalytic applications. However, due to a high tunability of the perovskite structure, this concept can be applied to practically any metal, which is able to adopt the coordination of the B-site cation within the perovskite structure and which is "unstable" at low oxygen partial pressures.

On the basis of lanthanum-doped strontium titanates, substituted with nickel, a self-regenerating effect can be induced to limit the microstructural degradation of the catalytically active phase while cleaning off the catalytic surface

suffering from poisoning. Conventionally prepared catalysts (Fig. 2) tend towards a substantial loss of the active surface area, either by coalescence from long-term exposure to high temperatures or from increased particle mobility at elevated water vapour pressures. With the here-presented material concept, the exsoluted metallic nickel phase can be renewed, by a chemical stimulus, in terms of oxygen partial pressure (Fig. 2a).

Assuming cyclic and fully reversible catalyst metal exsolution/integration, the oxidation of the material would then lead to the incorporation of the degraded metallic phase into the host perovskite. By knowing this, the authors propose a material based strategy for catalytic self-regeneration on top of the microstructural self-regeneration: at the same time, as the here-addressed microstructural self-regeneration takes place, it is expected that the surface can be cleaned off by the oxidation of poisoning species (i.e. sulfur species to SO_2 and C to CO_2) (Fig. 3). Subsequent to this, a regenerated catalytic phase is segregated from the host matrix during the reduction step. We address this idea as particularly attractive for technologies within the renewable energy sector: gas processing and power-to-gas technologies (methanation, steam reforming, etc.), as well as anodes for high temperature electro-catalysis in solid oxide fuel cells (SOFCs) and solid oxide electrolysis cells (SOECs), for which coarsening of the Ni phase takes place in state-of-the-art Ni/YSZ anodes and leads to severe performance loss.[8] In this case, Ni agglomeration will lead to de-percolation, which means that the electron pathways are interrupted by particle growth (Fig. 2). This results in a harmful increase of the ohmic resistance and significantly lowers the electrochemical activity.[8–11] Finally, in this study, we also report about a very low temperature but single-step powder synthesis technique. In contrast to conventional wet chemistry syntheses, high surface area powders obtained offer the application of these materials for other catalytic applications.
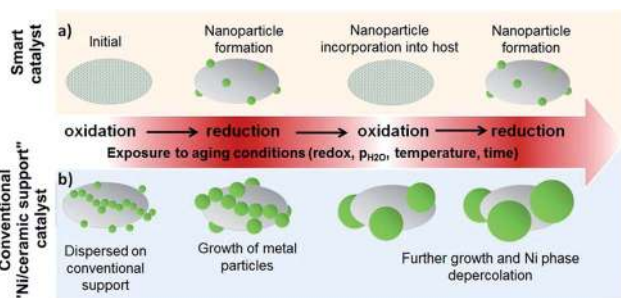

Fig. 2 The principle of microstructural self-regeneration compared to that of the degradation of conventional catalysts, e.g. nickel supported on a mixed oxide phase, adapted from Nishihata et al.[7]; the smart material microstructure is segregated during redox cycling, whereas the conventional nickel catalyst undergoes a harsh coarsening upon exposure to aging conditions.[11]

Materials and methods

Material synthesis

Materials were synthesized according to an in-house adapted citrate-gel method. Lanthanum(III) nitrate hexahydrate,
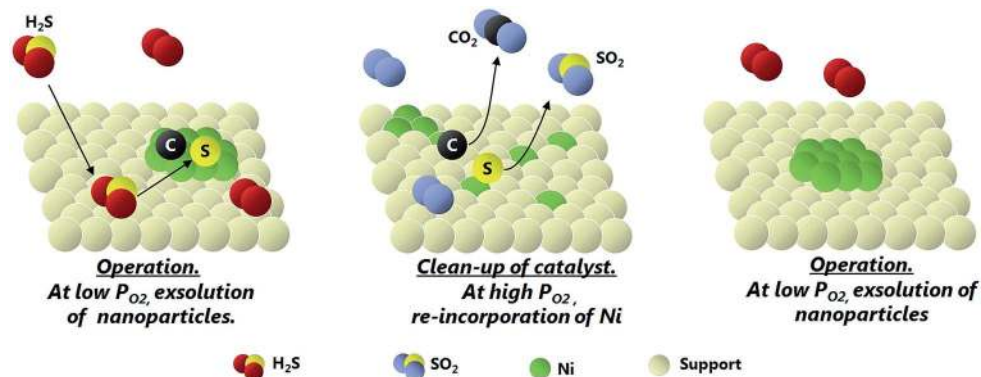

Fig. 3 A proposed clean-off procedure of a smart material catalyst triggered by redox cycling.

strontium(II) nitrate, nickel(II) acetate tetrahydrate, (Puriss, Fluka, Switzerland), and titanium diisopropoxide bis-acetylacetonate (Puriss, TBAD, Mateck, Germany) were used as starting precursors.

Stoichiometric amounts of the metal salts were dissolved in an aqueous solution of citric acid (CA, Puriss, Sigma-Aldrich, Switzerland) and ethylene diamine tetra-acetic acid (EDTA, Puriss, ABCR, Germany). An ammonia solution (25%, Sigma-Aldrich) was used as a pH controlling agent. The ratio of metal ions to CA to EDTA was 1 : 1.5 : 1. The compositions synthesized in this study follow the stoichiometry of $La_xSr_{1-3/2x}Ti_{1-y}Ni_yO_{3-\delta}$, (LSTN), for which the charge balance is maintained by introducing A-site vacancies. The sample denotations, used in this study and their corresponding stoichiometries, have been summarized in Table 1. After stirring, the precursor solution was placed in a drying furnace for 12 hours at 140 °C. The resulting foam was crushed and heat treated for 6 hours at 650 °C. In this work, we refer to this particular firing stage as "as-prepared", after which all organic components are burned off. The samples fired subsequently at 1000 °C are referred to in this work as "calcined".

Material characterisation

The samples were reduced, in a tube furnace, under a constant flow of 5 vol% H_2 for the exsolution of Ni from the perovskite host structure. The crystal structure and phase purity were determined for the pressed samples by X-ray diffraction (XRD) on a Bruker D8 Advance with Ni-filtered Cu radiation, variable slits and an energy sensitive line detector (LynxEye). The measurements were performed using tube settings of 40 kV/40 mA. The lattice parameters were determined by using the TOPAS software, with applied zero-shift correction. For thermogravimetric analysis (TGA), the calcined samples were pressed at approx. 7.5 kN·cm^{-2}, forming a porous pill. The pressed pills were heated at 5 K min^{-1} to 1100 °C under a reducing atmosphere (*ca.* 2.5% H_2/Ar) with a holding time of 2 h. Measurements were performed on a Netzsch STA/IR 449 C Jupiter and the resulting exhaust gases were analyzed with a Bruker Tensor 27.

Determination of the nickel particle size

The nickel particle size was calculated with the assumption that exsolved particles are represented by single crystallites, which can be determined by the Scherrer equation:

$$\tau = \frac{K\lambda}{\beta \cos \theta}$$

where τ – mean size of ordered crystalline domains in nm, K – dimensionless shape factor, λ – X-ray wavelength, and β – peak broadening at half maximum of the intensity.

The peak broadening β itself is defined as follows:

$$\beta = B_s - B_I - B_m$$

where B_s – contribution of nanoparticle size, B_I – instrumental contribution and B_m – microstrain contribution.

The instrumental peak profile was obtained from separate XRD data on an Al_2O_3 reference sample, delivered by Bruker. The possible contribution of a microstrain effect to the total peak broadening (β) was qualitatively inspected by Williamson–Hall plots in accordance with:

$$\beta(2\theta) = 4\varepsilon \frac{\sin \theta}{\cos \theta}$$

Peak broadening was determined by Rietveld refinement using Topas software (Bruker). The background of the experimental data was described by a fourth order polynomial function, whereas the peak profile was fitted with a pseudo-Voigt function. The fitting parameters were based on the Newton–Raphson least squares method.

Microstructure analysis and sample morphology analysis

Scanning electron microscopy (SEM) was performed on a Zeiss Supra 40VP with a field emission gun and a Bruker EDS detector. Powder samples (reduced and oxidized) were dispersed with isopropanol and deposited on conductive carbon stickers. To reduce charging, some of the powder samples were sputtered with gold. The EDS analyses were conducted on non-coated samples. TEM analysis has been conducted on powder samples, which were reduced for 2 and additionally for 12 hours at 900 °C. Powder samples were ultrasonically dispersed in isopropanol and deposited on a copper TEM grid. The TEM analysis was conducted with an FEI Technai F30, while STEM and energy filtered EDS mapping were carried out on a Hitachi STEM HD2700CS with a CEOS aberration corrector at acceleration voltages of 200 kV. The specific surface area (SSA) of powders was determined from a five-point nitrogen adsorption isotherm at 77 K by applying the Brunauer–Emmett–Teller (BET) theory. The powders were first dried for 2 hours at 180 °C, in a nitrogen flow, and then measured on a Quantachrome Nova 2000e.

Results and discussion

Low-temperature synthesis of Ni-doped titanates

The investigation of such nanoscale catalysts for this smart material concept requires a specific synthesis technique, which ensures high chemical purity and elemental homogeneity.

Larger inhomogeneities, in the molecular composition, would result in varying exsolution/reintegration behaviour.

Table 1 Denotation of LSTN materials and the corresponding stoichiometry

Sample denotation	Chemical formula	Ni : La ratio [at%]
LST27-0Ni	$La_{0.2}Sr_{0.7}TiO_{3-\delta}$	0 : 20
LST35.5-0Ni	$La_{0.3}Sr_{0.55}TiO_{3-\delta}$	0 : 35
LST44-0Ni	$La_{0.4}Sr_{0.4}TiO_{3-\delta}$	0 : 40
LST27-5Ni	$La_{0.2}Sr_{0.7}Ti_{0.95}Ni_{0.05}O_{3-\delta}$	5 : 20
LST35.5-5Ni	$La_{0.3}Sr_{0.55}Ti_{0.95}Ni_{0.05}O_{3-\delta}$	5 : 35
LST44-5Ni	$La_{0.4}Sr_{0.4}Ti_{0.95}Ni_{0.05}O_{3-\delta}$	5 : 40

This journal is © The Royal Society of Chemistry 2016

J. Mater. Chem. A, 2016, **4**, 11939–11948 | **11941**

However, our own experiments[12,13] and a complementary literature survey on the synthesis of such co-substituted titanate materials[14–20] allow only one conclusion: the synthesis of phase pure LSTN is challenging due to the high calcination temperatures necessary to form the titanate host structure and the additional rival formation of meta-stable perovskite phases, as well as a slow diffusion of La/Sr elements into the titania lattice.

Most of the conventional processes, like solid state reactions, need very high calcination temperatures above 1400 °C, in combination with repetitive calcination and grinding steps, which often introduce contaminations.[12] Such synthesis routes are economically unsuitable, as well as being unsuitable for the production of highly pure and homogeneous materials. In one of the previous studies, the authors have circumvented these problems by a nanoparticle based spray pyrolysis process.[12,13] Titania nanoparticles and inorganic salts were used as reagents, hence overcoming the problem of slow diffusion kinetics. Although this synthesis route allowed the production of single phase materials at temperatures as low as 1200 °C, it still required grinding procedures to achieve a sufficiently high surface area.

The results of this synthesis and related crystal structure patterns, in the as-prepared state, as well as after calcination, are compared in Fig. 4. The desired and expected single phase perovskite structures are obtained for the nickel-free ternary (LST), as well as for the nickel-containing quaternary (LSTN) perovskite compositions, after an initial burnout of organic compounds for 6 h at 650 °C (Fig. 4a). Rietveld refinement of these diffraction patterns confirmed the existence of single phase cubic structures ($Pm3m$) for all compositions. The formation of perovskite phases at such low temperatures is likely due to the additional combustion enthalpy from EDTA in combination with its function as a stabilizing complexing agent for the cation elements at the atomic scale. In such a homogeneously mixed precursor, nearly no diffusion limitations exist between the cations. Such low temperatures are not reported yet for such complex titanate compositions, but they are crucial for keeping a high SSA for an effective catalytic performance.

The application of a rather low calcination temperature was found to have an impact on the maximum nickel content, which can be incorporated into the perovskite structure. Exclusively phase pure XRD patterns were recorded after a single step calcination at 1000 °C for stoichiometries up to 5 at% of nickel. But for compounds with 5 to 10 at% of nickel, secondary NiO and $NiTiO_3$ phases were detected, which indicate a solubility limit of nickel in the titanate framework as a function of temperature. However, more detailed XRD analyses show the influence of nickel doping on the cubic lattice parameter (Fig. 5). At low calcination temperatures of about 1000 °C and for nickel contents up to 10 at%, the lattice parameter expands as a consequence of the substitution of Ti by the larger nickel ions ($IR_{Ti^{4+}(VI)} = 0.605$ Å, $IR_{Ni^{2+}(VI)} = 0.690$ Å). This implies a slow diffusion of nickel into the perovskite host structure and the incorporation of larger amounts of nickel probably requires a greater energy input by means of harsher heat treatment conditions. Subsequent experiments, under harsher conditions, namely calcination for 12 hours at 1400 °C, have proven
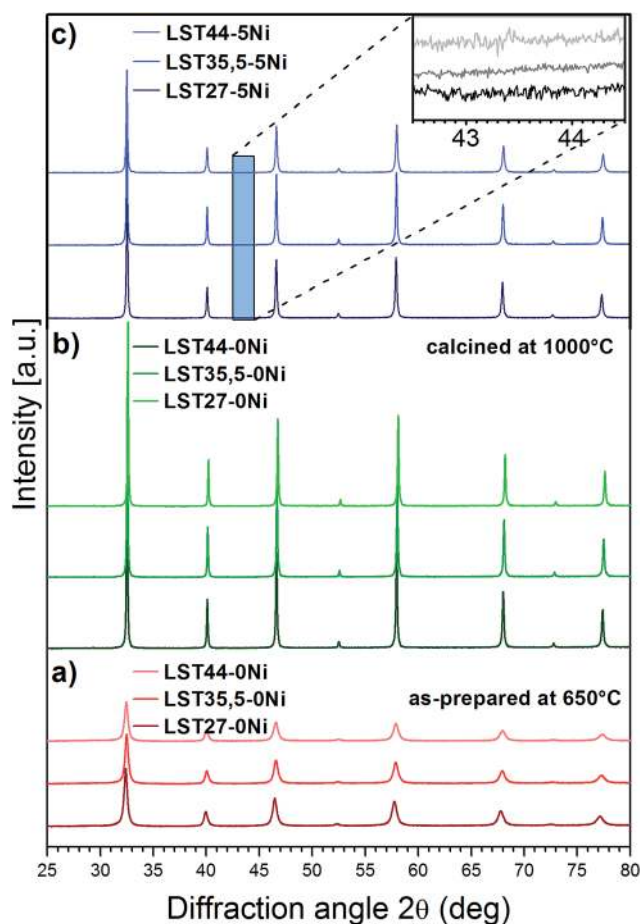

Fig. 4 XRD patterns of the synthesized powders: LST-0Ni under the as-prepared conditions (a), LST-0Ni after calcination at 1000 °C (b), and LST-5Ni after calcination at 1000 °C (c) with an inset of the 42.5–44.5 2θ range. The absence of NiO related (200) peak at 2θ 43.276° indicates the phase purity and the integration of nickel into the host structure of LST.
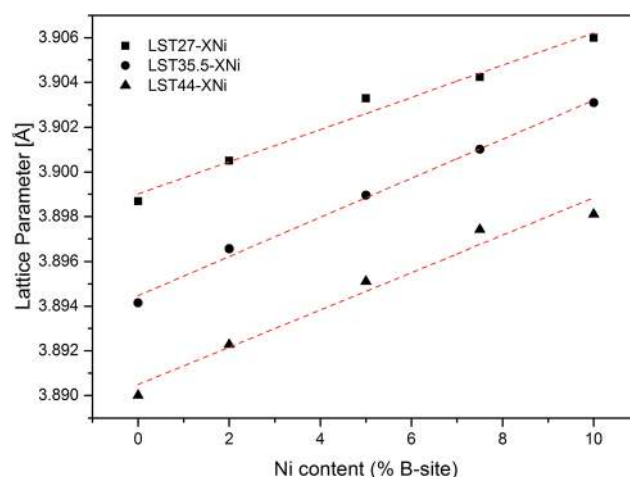

Fig. 5 Lattice parameters of three LSTN materials (LST27-XNi, LST35.5-XNi, LST44-XNi, where X denotes the content of Ni in at%) with varying amounts from 0 to 10 at% of Ni substitution. All compositions were calcined at 1000 °C and the lattice parameters are the average values of three measurements. Error bars are smaller than the symbols.

that it is possible to prepare phase pure LSTN with 10 at% of nickel. Similar results with respect to the applied temperature are given in the literature, when multi-step solid state synthesis procedures at high temperatures were applied for LSTN.[5,6,21] Keeping in mind that a typical SOFC or SOEC device is operated at about 900 °C or even lower, a full reintegration of nickel species into the perovskite host matrix should be targeted at a reoxidation temperature of less than 1000 °C. Therefore, LSTN compositions with up to 5% nickel are considered promising materials for the mentioned applications. The question whether only a partial reintegration of the nickel is sufficient for the aimed catalytic self-regeneration is currently under investigation. However, the basic methodology is proven here.

Material concept for catalytic applications

In contrast to existing high temperature syntheses, which exclusively lead to the formation of particles in the micron range, the here-synthesised materials preserve a high surface area in the "as-synthesized" state, *i.e.* even after a heat treatment at 650 °C. This can be seen from the peak broadening in the XRD data (Fig. 4a) and BET measurements, from which SSA values of 25–30 m^2 g^{-1} ($d_{50BET} \sim$ 30 nm) were determined. Further calcination at 1000 °C leads to a narrowing of the peaks (Fig. 4b and c) and loss of the SSA down to 8–12 m^2 g^{-1}. However, with a d_{50BET} of around 80 nm, the BET equivalent particle diameter still remains within the nanosize range. Hence, with this advantageous synthesis route, additional grinding steps become redundant and potential material contaminations can be avoided. From the TEM analysis of the

particles after a calcination step at 900 °C (Fig. 6a) and prolonged aging under reducing 5 vol% H$_2$ in Ar (Fig. 6b), two distinct features can be identified: first, the perovskite host particle, with a rather low contrast, and secondly, spherical and dark nickel nanoparticles. It is evident from the elemental mapping in Fig. 6c that the latter and dark nanostructures consist solely of nickel. This is direct and conclusive evidence of selective exsolution from the LSTN perovskite host structure. The coarsening of such fine particles is expected to occur under these conditions (Fig. 2, bottom).[5,9] Images representing both materials before (Fig. 6a) and after (Fig. 6b) a prolonged high temperature aging for 12 hours show a similar nickel nanoparticle diameter of about 20 nm and prove a certain extent of stability of the exsoluted nickel particles.

It is also worth highlighting that the presented STEM images and correlated energy filtered EDS analysis evidence a very uniform distribution of Sr and Ti, indicating a high chemical homogeneity.

With respect to the potential, future application, good stability and preservation of high SSA are given. The smart material concept presented here is particularly attractive for processes, where high SSA catalytic particles under reducing conditions play an important role, *e.g.* processes such as hydrocarbon cracking and methanation, but also the reforming and production of synthetic fuels.

Material concept for novel SOFC anodes

In conventional SOFC anodes, high Ni contents (higher than the percolation threshold) are used because Ni is not only used as
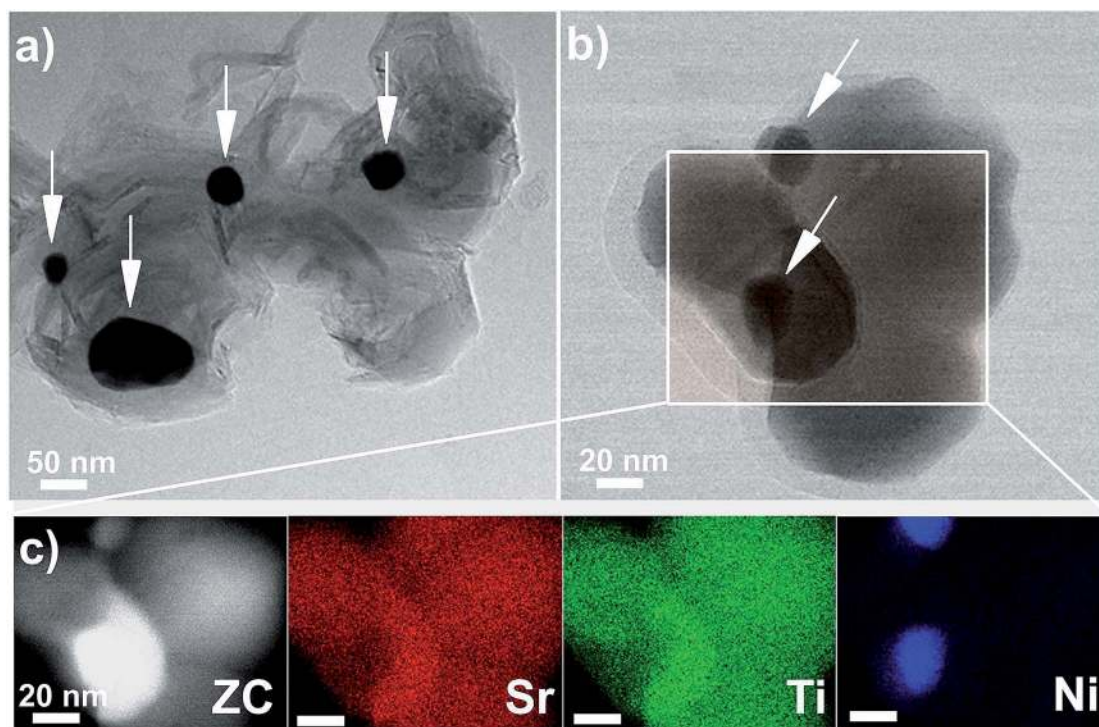

Fig. 6 Microstructure and morphology of the formed nanostructured catalyst: transmission electron microscopy image of LST-5Ni nanoparticles reduced for 2 hours at 900 °C (a), phase contrast image of LST-5Ni with the marked investigated area detailed after 12 hour reduction at 900 °C (b), and HR-STEM z-contrast (ZC) image and energy filtered EDS mapping showing selectively Sr, Ti and Ni distribution (c).

a catalyst but it also represents the electronic conducting phase. Unfortunately, high Ni-contents are the reason for significant degradation associated with agglomeration at high operating temperature and volume changes upon redox cycles. Thus, new material concepts were introduced with a ceramic mixed conducting phase (*e.g.* CGO). It was shown that these anodes can reach high performance with Ni-contents as low as 3%.[22] Since LSTN is an electronic conductor, we particularly address this smart material concept of an anode catalyst for novel SOFC and SOEC electrodes.[3,14] In this context, the concept of smart catalysts becomes very important, in order to avoid the poisoning of the reduced Ni-surface and to maintain the nanosized dimensions. In addition, Ni undergoes significant volume change upon oxidation. In particular for composite materials with a high Ni-content (such as Ni-YSZ anodes), the Ni to NiO transformation is the reason for severe degradation leading also to mechanical instability. With the new material concept and with the smart catalyst, the redox process – causing an unavoidable degradation of Ni-YSZ and finally a total failure of the cell – can actively be used now as a regenerating mechanism.

From the very limited information on metal exsolution from titanate perovskites, it can be assumed that the exsolution of a metallic phase from the perovskite host matrix depends on the surface condition and quality, whereby cleaved and pristine surfaces provide a better support for the nucleation and formation of exsoluted nanoparticles than aged surfaces.[21] To investigate this, LSTN compositions with various A-site deficient stoichiometries and with varying surface conditions were investigated with respect to the resulting morphology and microstructure after a reduction for 2 h at 900 °C in 5 vol% H_2 in Ar (Fig. 7). After reduction, multiple nanostructured nickel particles appear on terminated (native) as well as on pre-polished surfaces. Nickel appears as bright particles on the surface of the darker
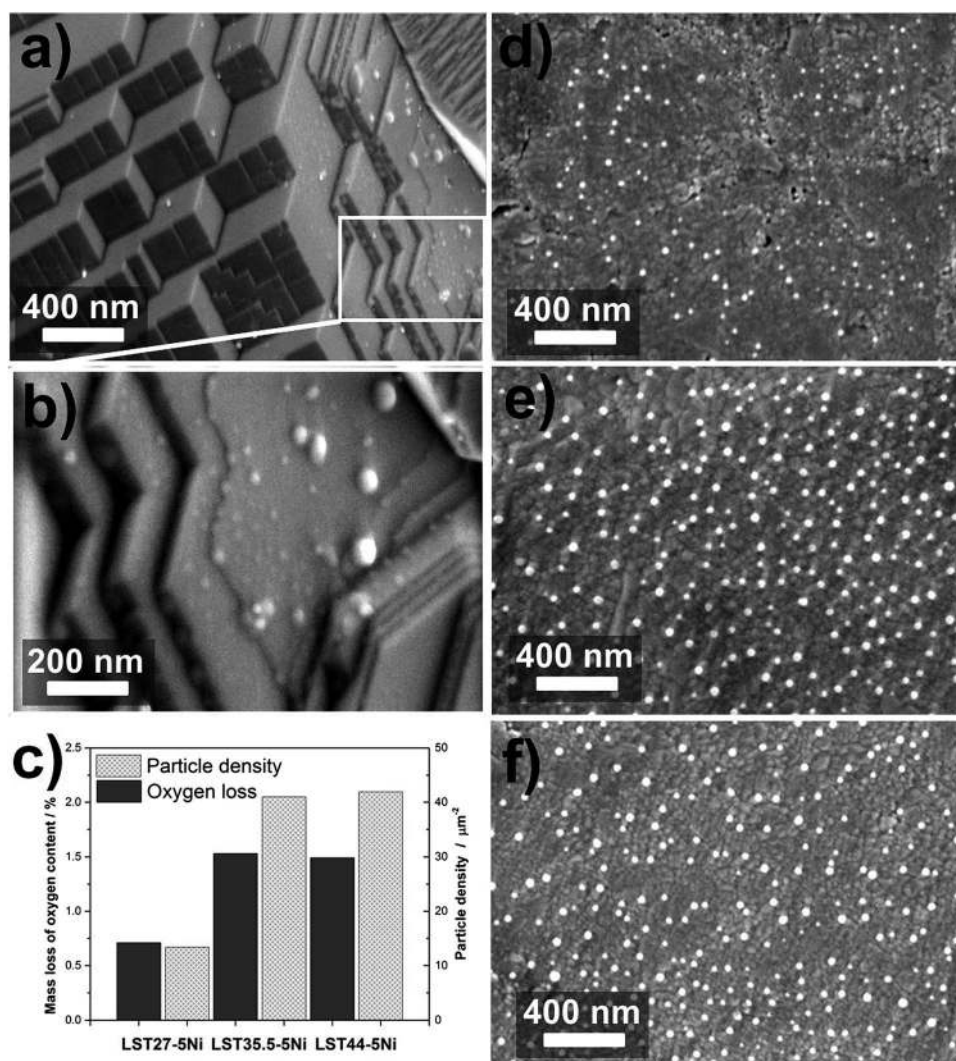

Fig. 7 Microstructure of LSTN samples after reduction and exsolution of nickel: untreated and original LST27-5Ni surfaces with terraces and exsoluted nickel particles (a and b). Comparison of the oxygen loss of the perovskite during reduction and the resulting nickel particle density as number per surface area in μm^2; comparison of particle density measured from the polished surfaces with the oxygen loss determined by the use of TGA analysis (c), SEM images of the pre-polished and reduced surfaces of LST27-5Ni (d), LST35.5-5Ni (e) and LST44-5Ni (f). Study conducted on dense bulk specimens.

11944 | *J. Mater. Chem. A*, 2016, 4, 11939–11948

This journal is © The Royal Society of Chemistry 2016

LSTN due to the higher z-contrast of nickel. The nanoparticle population on the polished surfaces is much greater than on the native (original) surfaces, which matches the observation made elsewhere.[5] This effect is not yet well understood and clearly requires a future in-depth analysis to determine surface termination effects. However, a possible explanation could be given by a predominantly A-site terminated surface or a surface close to stoichiometry variation, such as titanium enrichment or nickel depletion due to nickel volatilization during sintering.[23–25] It has to be mentioned that only larger nanoparticle clusters could be easily identified and visualized due to the angular resolution of the SEM. Indeed, a more specific and careful SEM analysis revealed the existence of much smaller clusters at the exsolution-preferred terrace steps, which is also attributed to very small nickel particles (Fig. 7b). With respect to the addressed novel

SOFC anode concept, the LSTN phase itself provides the electronic conductivity within the electrode microstructure. Hence, the amount of electronic conductive nickel can be substantially reduced by a factor of 10 to serve only as a catalyst. From this point of view, already the amount of nanoparticles documented in Fig. 7 seem to provide more than sufficient exposed active surface for the above mentioned applications. The specific characterization of the catalyst activity in the powder form and when used in the application (*e.g.* as SOFC anodes) is currently performed and will be the issue of a follow up paper. For the correlation of material stoichiometry and nickel exsolution efficiency, pre-polished surfaces were investigated with respect to the amount of exsoluted nickel particles after reduction. It is quite obvious, that a larger amount of nickel is exsoluted from titanates with higher A-site deficiency and this is again correlated
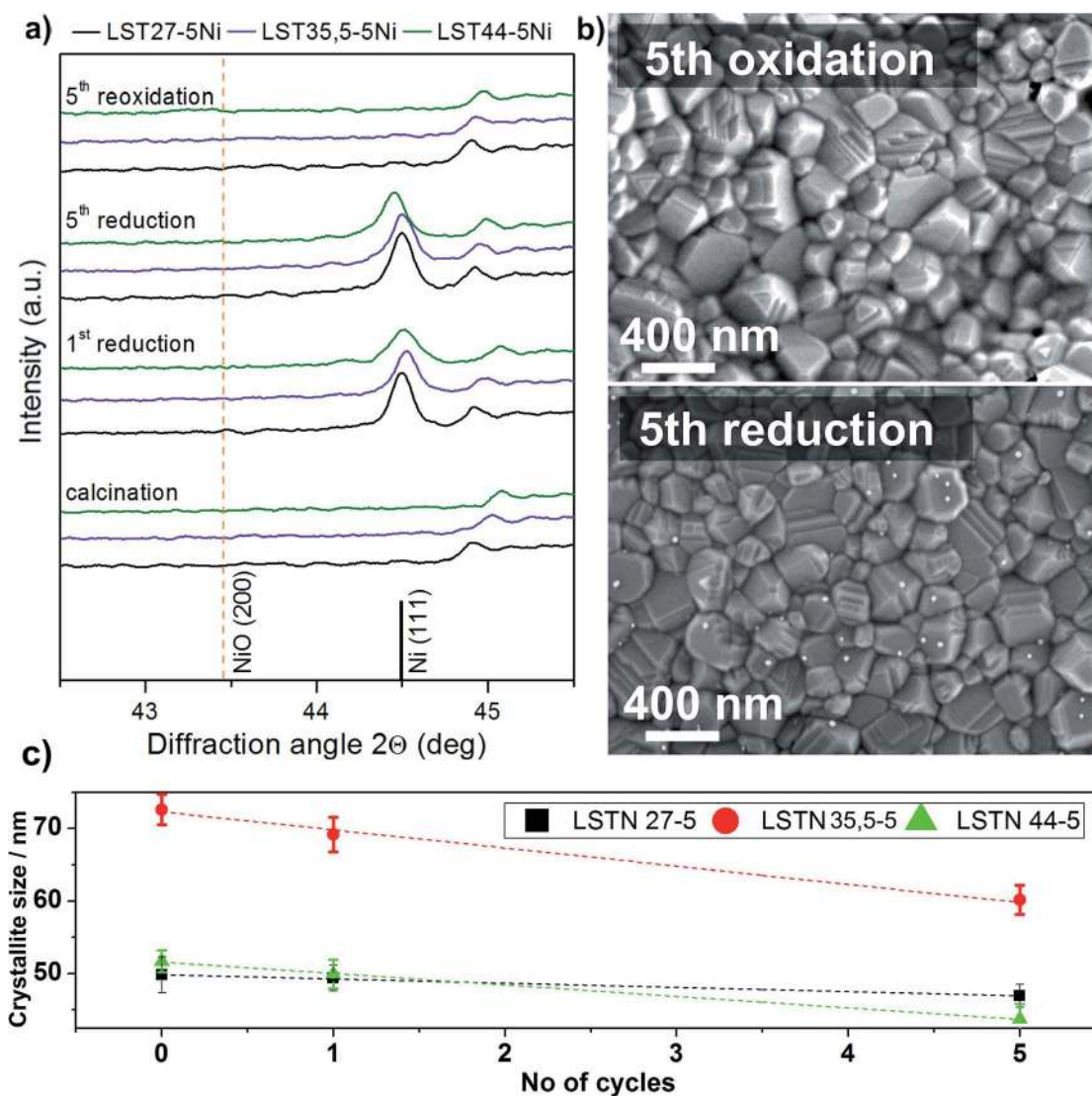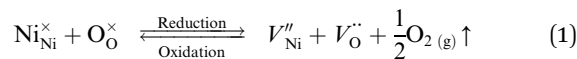

Fig. 8 Comparison of crystal structure and microstructural changes caused by redox cycling. Reversibility of the crystal structure upon 5 redox cycles by XRD (a). The diffraction pattern focuses on the 2θ range of Ni and NiO. Comparison of a representative LSTN–5Ni surface after 5th oxidation ((b), top) and 5th reduction step ((b), bottom): exsolution of nickel after oxidation and reintegration of formed nickel clusters after the reduction. Comparison of the average crystallite size of the exsoluted Ni phase (c). Study conducted on powdered specimens. Total high temperature treatment time under reducing conditions: 72 hours at 900 °C.

This journal is © The Royal Society of Chemistry 2016

J. Mater. Chem. A, 2016, **4**, 11939–11948 | **11945**

with the oxygen loss in the perovskite (Fig. 7c). A-site deficiency is expected to destabilize the perovskite structure and lead to higher oxygen loss from the lattice, which in turn is associated with larger extents of nickel exsolution. This can be explained by the following formula, whereby nickel in the host structure is being exsoluted:

$$Ni_{Ni}^{\times} + O_{O}^{\times} \underset{\text{Oxidation}}{\overset{\text{Reduction}}{\rightleftarrows}} V_{Ni}'' + V_{O}^{\cdot\cdot} + \frac{1}{2}O_{2\,(g)}\uparrow \qquad (1)$$

Similar conclusions have been drawn from quantitative analysis of the nickel phase in the XRD data. Hence, highly A-site deficient compositions are preferred for SOFC and SOEC applications, if a self-regeneration effect is aimed at. Finally, we want to highlight the potential of this material concept if LSTN compositions with greater metal substitution are developed. Having restricted the heat treatment to low temperatures in order to preserve high particle surface area, we concentrated in this work on solid Ni solutions having up to 5 at% of Ni. Literature survey reports single phase LSTN compositions with Ni contents as high as 25 at%, which suggests that also higher contents of surface Ni could be obtained.[6]

Microstructural reversibility and thermal stability of the Ni phase

Neagu et al.[5,21] have shown that exsolution of a metallic phase such as nickel from a titanate perovskite host matrix is possible and that this concept can be used to prepare nanoparticles on the surface. However, it was not shown that this material effect could be used in a reversible manner by reintegrating the metallic phase in the host titanate and to apply this effect repetitively, and on purpose, for microstructural and catalytic self-regeneration. To support the self-regeneration concept, a series of microstructural analyses, in combination with powder XRD, were carried out to prove the reversibility of the here-investigated material compositions. The changes in the crystal structure itself, as well as on the microstructure surface, are shown on LSTN samples, subjected to 5 redox cycles at 900 °C (Fig. 8).

It is clearly evident from the diffraction data that all three investigated compositions form a metallic nickel phase upon exposure to a reducing environment. The formation of nanostructured nickel clusters on the surface of the perovskite is supported by SEM analyses of the microstructure (Fig. 8b, bottom). Upon exposure to a p_{O_2} value as is typical for air, the reflections attributed to the nickel phase (Ni 111) disappear and nickel particles are no longer observed on the surface of LSTN. Simultaneously, the lattice parameter of the main perovskite phase changes reversibly upon the reduction/oxidation (see Fig. S1 in the ESI†). The effect of the lattice expansion/shrinkage is however not pronounced and is assumed to reflect Ni and O loss, lattice expansion due to Ti reduction and some possible interstitial Ni trapped within the lattices. All of the above observations clearly prove a reversible and complete conversion of the microstructure and the crystal structure. For an incomplete integration of exsoluted nickel particles or clusters into the LSTN framework, the formation of NiO with reflections at

a 2 value of 43.276° is expected.[26] Nevertheless, after the fifth reoxidation, no evidence of the NiO 200 peak is given, which again supports a fully reversible exsolution and reincorporation mechanism of nickel (Fig. 8a).

The newly formed nickel phase features very characteristic and nanoparticle related peak shapes with a broad full-width at half maximum (FWHM). This is similar to the nanoparticle samples discussed in the previous section and is correlated with the formation of nanostructured scattering domains. The analysis of FWHM evolution of the Ni (111) peak over the redox cycling (Fig. 8c) confirms our tentative TEM observations concerning the excellent thermal stability of Ni nanoparticles. From Fig. 8c it can be seen that as the redox cycles continue, not only do the newly formed crystallites not grow, but actually seem to slightly decrease in size. This effect will be further studied in detail and supports our smart material concept, in which a redox stimulus is used to regenerate the microstructure and to prevent the growth of the catalytically active phase.

Outlook

The proposed concept can be applied to various processes in which varying oxygen partial pressures can be used for microstructural self-regeneration. Here, nickel is highlighted as to show the potential of this innovative approach for high temperature fuel cell systems, but other material combinations of a catalytically active phase and perovskite host compositions are possible. The validation of the here-proposed LSTN and the involved reversibility of the structural change indicate that this material effect is a powerful concept to regenerate blocked or even poisoned catalysts by a simple change of the oxygen partial pressure and at the same time, microstructural regeneration, which provides again fresh nanostructured clusters of the catalytic phase. Redox cycling commonly causes an unavoidable structural and catalytic degradation of the state-of-the-art Ni/YSZ and finally a total cell failure.[9] The application of such perovskite materials, as proposed here, allows a proactive regeneration of the catalytically active materials in SOFC or SOEC electrodes as well as of materials used in more conventional catalysis. In the case of titanate-based perovskites, this self-regeneration effect could be applied to limit microstructural and catalytic degradation. Redox cycling stimulates first the incorporation of the degraded metallic phase into the perovskite, while this structural change is accompanied by a total oxidation of impurities, e.g. deposited sulfur species to SO$_2$ and carbon depositions to CO$_2$. Afterwards, when changing back to reducing conditions, the segregation of a regenerated, nanostructured and highly dispersed, catalytically active phase follows. The authors currently focus their research on the understanding and the precise control of catalytic regeneration and how operation conditions influence the nanoparticle size, size distribution and population.

Conclusions

A smart material concept for a self-regenerating catalyst, based on lanthanum-doped strontium titanates, substituted with

nickel as catalytically active element is proposed. Phase pure perovskite-type LSTN was synthesized by a modified citrate route at a very low temperature of 650 °C. This allowed the preservation of the high specific surface area of the particles and avoided the need for further processing and conditioning steps. Furthermore, smaller particles do not limit the exsolution of the catalytically active element due to the potentially critical diffusion path lengths. The formation of nanostructured nickel clusters appears to be dependent on the surface conditions of the reduced host material as well as on the A-site under stoichiometry of LSTN. A higher A-site deficiency leads to larger amounts of exsoluted nickel. The exsolution and especially the subsequent reintegration of nickel domains were found to be reversible and repetitive under continuous redox cycling. This validates the proposed smart material concept for the self-regeneration of poisoned catalysts *via* redox cycling. Furthermore, the good electronic properties make LST-based catalysts especially attractive for solid oxide fuel cell anodes. However, these materials are also applicable to any other catalytic applications under reducing conditions for which the regeneration of a catalyst can be necessary due to catalyst poisons such as the synthesis of renewable CH_4 fuels by CO_2 methanation.

Acknowledgements

References

1 M. D. Argyle and C. H. Bartholomew, Heterogeneous Catalyst Deactivation and Regeneration: A Review, *Catalysts*, 2015, **5**(1), 145–269.

2 A. K. Neyestanaki, *et al.*, Deactivation of postcombustion catalysts, a review, *Fuel*, 2004, **83**(4–5), 395–408.

3 D. K. Niakolas, Sulfur poisoning of Ni-based anodes for Solid Oxide Fuel Cells in H/C-based fuels, *Appl. Catal., A*, 2014, **486**, 123–142.

4 Y. Nishihata, *et al.*, Self-regeneration of a Pd-perovskite catalyst for automotive emissions control, *Nature*, 2002, **418**(6894), 164–167.

5 D. Neagu, *et al.*, *In situ* growth of nanoparticles through control of non-stoichiometry, *Nat. Chem.*, 2013, **5**(11), 916–923.

6 C. Arrivé, *et al.*, Exsolution of nickel nanoparticles at the surface of a conducting titanate as potential hydrogen electrode material for solid oxide electrochemical cells, *J. Power Sources*, 2013, **223**, 341–348.

7 Y. Nishihata, *et al.*, Self-regeneration of a Pd-perovskite catalyst for automotive emissions control, *Nature*, 2002, **418**, 164–167.

8 L. Holzer, *et al.*, Microstructure degradation of cermet anodes for solid oxide fuel cells: Quantification of nickel grain growth in dry and in humid atmospheres, *J. Power Sources*, 2011, **196**(3), 1279–1294.

9 B. Iwanschitz, *et al.*, Nickel agglomeration in solid oxide fuel cells: The influence of temperature, *Solid State Ionics*, 2012, **211**(0), 69–73.

10 L. Holzer, *et al.*, Quantitative relationships between composition, particle size, triple phase boundary length and surface area in nickel-cermet anodes for Solid Oxide Fuel Cells, *J. Power Sources*, 2011, **196**(17), 7076–7089.

11 B. Iwanschitz, *et al.*, Degradation of SOFC Anodes upon Redox Cycling: A Comparison Between Ni/YSZ and Ni/CGO, *J. Electrochem. Soc.*, 2010, **157**(2), B269–B278.

12 D. Burnat, *et al.*, Synthesis and performance of A-site deficient lanthanum-doped strontium titanate by nanoparticle based spray pyrolysis, *J. Power Sources*, 2012, **201**, 36.

13 D. Burnat, *et al.*, On the chemical interaction of nanoscale lanthanum doped strontium titanates with common scandium and yttrium stabilized electrolyte materials, *Int. J. Hydrogen Energy*, 2012, **37**(23), 18341.

14 D. Neagu and J. T. S. Irvine, Structure and Properties of $La_{0.4}Sr_{0.4}TiO_3$ Ceramics for Use as Anode Materials in Solid Oxide Fuel Cells, *Chem. Mater.*, 2010, **22**(17), 5042–5053.

15 J. Canales-Vázquez, *et al.*, Studies on the reorganisation of extended defects with increasing n in the perovskite-based $La_4Sr_{n-4}Ti_nO_{3n+2}$ series, *Adv. Funct. Mater.*, 2005, **15**, 1000–1008.

16 J. Canales-Vazquez, W. Zhou and J. T. S. Irvine, Characterisation of novel anodes for solid oxide fuel cells based on oxygen-excess perovskite related structures, *Solid State Ionics*, 2002, **8**(3–4), 252–255.

17 A. D. Aljaberi and J. T. S. Irvine, Ca-substituted, A-site deficient perovskite $La_{0.2}Sr_{0.7}TiO_3$ as a potential anode material for SOFCs, *J. Mater. Chem. A*, 2013, **1**(19), 5874.

18 M. C. Verbraeken, *et al.*, Evaluation of Ca doped $La_{0.2}Sr_{0.7}TiO_3$ as an alternative material for use in SOFC anodes, *J. Electrochem. Soc.*, 2012, **159**(11), F762.

19 O. A. Marina, N. L. Canfield and J. W. Stevenson, Thermal, electrical, and electrocatalytical properties of lanthanum-doped strontium titanate, *Solid State Ionics*, 2002, **149**(1–2), 21–28.

20 D. Neagu and J. T. S. Irvine, Enhancing Electronic Conductivity in Strontium Titanates through Correlated A and B-Site Doping, *Chem. Mater.*, 2011, **23**(6), 1607–1617.

21 J. Myung, *et al.*, *In situ* tailored nickel nano-catalyst layer for internal reforming hydrocarbon fueled SOFCs, in *14th International Symposium on Solid Oxide Fuel Cells*, SOFC 2015, Electrochemical Society, 2015, pp. 1121–1128.

22 S. Primdahl and M. Mogensen, Mixed conductor anodes: Ni as electrocatalyst for hydrogen conversion, *Solid State Ionics*, 2002, **152–153**, 597–608.

23 F. Sanchez, C. Ocal and J. Fontcuberta, Tailored surfaces of perovskite oxide substrates for conducted growth of thin films, *Chem. Soc. Rev.*, 2014, **43**(7), 2272–2285.

24 M. Burriel, *et al.*, Absence of Ni on the outersurface of Sr doped La_2NiO_4 single crystals, *Energy Environ. Sci.*, 2014, **7**(1), 311–316.

25 F. A. Rabuffetti, P. C. Stair and K. R. Poeppelmeier, Synthesis-Dependent Surface Acidity and Structure of $SrTiO_3$ Nanoparticles, *J. Phys. Chem. C*, 2010, **114**(25), 11056–11067.

26 S. Sasaki, K. Fujino and Y. Takeuchi, X-ray determination of electron-density distribution in oxides, MgO, MnO, CoO and NiO, and atomic scattering factors of their constituent atoms, *Proc. Jpn. Acad., Ser. B*, 1979, **55**, 43–48.